

EXPERIMENTAL ANALYSIS OF BEAM-TO-COLUMN JOINTS EQUIPPED WITH SPRAYED ALUMINIUM FRICTION DAMPERS

Massimo Latour^{a*}, Vincenzo Piluso^a, Gianvittorio Rizzano^a

^aUniversity of Salerno, Dept. of Civil Engineering, Italy
mlatour@unisa.it, v.piluso@unisa.it, g.rizzano@unisa.it

ABSTRACT

In this paper, the results of an experimental analysis regarding beam-to-column joints equipped with friction dampers is presented. Even though the overall concept is not new, the connection structural detail and the friction pad material are different from previous proposals. In particular, the beam is connected to the column with a classical fixed T-stub fastening the upper flange and a friction damper located at the beam lower flange. The friction damper is composed of a stack of steel plates conceived to assure symmetrical friction. The friction pads are made of steel plates coated with thermally sprayed aluminium. The friction damper is designed in order to slide for a force level equal to or lower than the ratio between the nominal flexural resistance of the connected beam and the lever arm, i.e. the distance between the top T-stub and the friction damper. In this way, it is possible to obtain connections able to dissipate the seismic input energy almost without any damage to the steel elements, provided that all the joint components are designed with sufficient over-strength with respect to the actions corresponding to the friction damper sliding force. In this paper, such approach is validated reporting the results of an experimental campaign.

Keywords: Friction dampers, Connections, Free from yielding, Sprayed Aluminum

1. INTRODUCTION

The design of modern seismic resistant structures is based on a preliminary selection of the zones which have to be designed to assure the dissipation of the earthquake input energy. Dealing with Moment Resisting Frames (MRFs), the location of such dissipative zones at the beam ends is commonly preferred by adopting full-strength beam-to-column joints [1,2] which have to be designed with sufficient over-strength with respect to the connected beams. The required over-strength is aimed to assure the beam end yielding despite of the influence of random material variability [3,4] and the amount of strain-hardening occurring before the complete development of the ultimate flexural resistance of plastic hinges [5,6].

To date, the classical design philosophy based on weak beam-strong column-strong joint hierarchy has been widely applied in practical seismic design and surely provides some advantages, such as the development of stable hysteresis loops [7-10] and the prevention of soft-storey mechanisms which have to be avoided because of their poor energy dissipation capacity [11]. However, some drawbacks occur within the framework of the traditional design approach. On one hand, the use of full-strength beam-to-column joints with the code required over-strength can lead to the detailing of expensive structural connections which require the use of continuity plates, supplementary column web plates, reinforcing ribs or cover plates or, even, the use of haunched beams. On the other hand, also the overall frame design is costly, because of the column over-strength required to fulfil the strength hierarchy criteria, particularly in the case of long span beams, whose size is governed by gravity loads [12-15].

In order to overcome the drawbacks related to the use of full-strength beam-to-column joints, the use of partial-strength connections has been suggested and Eurocode 8 [1] has opened the door to their use provided that their plastic rotation capacity is properly demonstrated. Such design approach can be faced within the framework of the component approach [15-18]. The fastening elements of the beam-to-column joints have to be properly designed by selecting the weakest joint component, acting as dissipative component, and providing all the other joint components with sufficient over-strength. Moreover, the weakest joint component has to be designed to assure a ductile behaviour and the required plastic deformation capacity [19].

In last decades the application of partial strength joints to MRFs has been proposed and supported by a high number of research programs, both theoretical and experimental, devoted to characterise the behaviour of connections under monotonic [20-22] and cyclic loading conditions [23-27]. Nevertheless, even though the effort provided by the scientific community has been significant, there are still some issues which deserve further

59 investigation, such as the codification of design criteria for dissipative joints or the
60 development of new types of dissipative connections easy to replace or not requiring
61 replacement after a severe seismic event [28-31].

62 However, independently of the use of either full-strength or partial-strength beam-to-column
63 joints, the main drawback of the traditional seismic resistant design strategy is intrinsic in the
64 strategy itself. In fact, on one hand the structural damage is essential to dissipate the
65 earthquake input energy but, on the other hand, it is the main source of direct and indirect
66 losses. For this reason, many researchers have focused their attention on the strategy of
67 supplementary energy dissipation with the aim to reduce the structural damage under
68 destructive seismic events and, as a consequence, the direct and indirect losses. This strategy
69 is based on the use of energy dissipation devices which have to be inserted between couples
70 of points of the structural scheme where high relative displacements or velocities occur under
71 the action of severe ground motions [33-36]. Such displacements or velocities are expected to
72 activate specifically designed passive energy dissipation systems based on simple
73 mechanisms such as hysteresis, friction or viscosity of fluids.

74 Starting from the background briefly summarized above, in order to overcome the drawback
75 of the traditional design approaches, research efforts have been recently devoted to the
76 practical development of a new design strategy whose goal is the design of connections able
77 to withstand almost without any damage not only frequent and occasional seismic events, but
78 also destructive earthquakes such as those corresponding to rare and very rare events.

79 The concept behind this research is inspired to the strategy of supplementary energy
80 dissipation, but it is based on the use of damping devices under a new perspective. In fact,
81 while passive control strategies have been commonly based on the integration of the energy
82 dissipation capacity of the primary structure by means of a supplementary dissipation coming
83 from damping devices; conversely, the new design strategy is based on the use of friction
84 dampers conceived in such a way to substitute the traditional dissipative zones of MRFs, i.e.
85 the beam ends. To this scope, beam-to-column connections can be equipped with friction
86 dampers which can be located either at the level of the two flanges [37-39] or at the bottom
87 flange level only [40-42]. Also the beam web to column flange connection can be equipped
88 with friction dampers. Moreover, symmetrical [39, 43] or asymmetrical friction devices can be
89 exploited [35, 38].

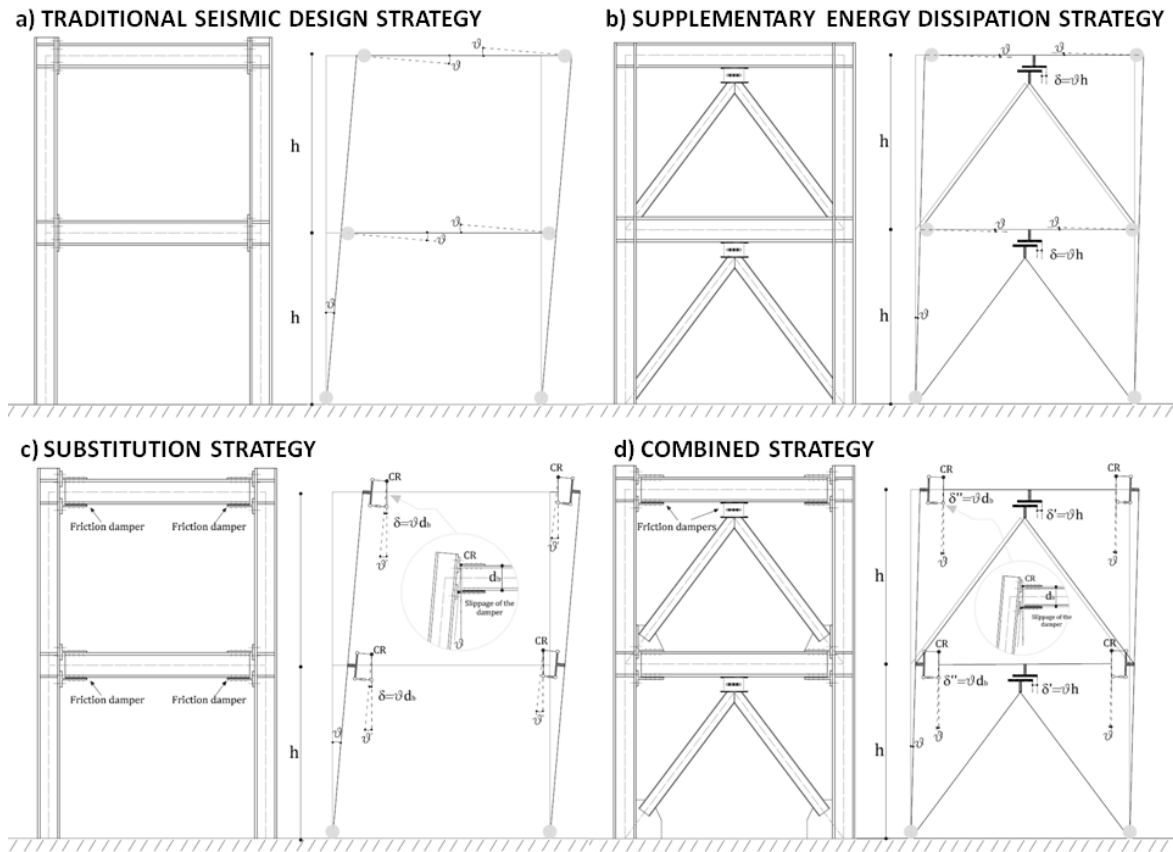


Figure 1: Comparison between different design strategies

90

91 In order to well clarify the aim of the work, its framework and the differences with either
 92 traditional seismic design or supplementary energy dissipation strategy, the different
 93 schemes are analysed in Fig. 1. In particular, Fig. 1a points out that dissipative zones of
 94 traditional MRFs are located at the beam ends where plastic hinges have to be developed. The
 95 seismic demand is usually expressed in terms of maximum interstorey drift (ϑ in the figure)
 96 which governs the plastic rotation expected in dissipative zones. The supplementary energy
 97 dissipation strategy (Fig. 1b) is aimed to the reduction of the seismic demand by introducing
 98 seismic dampers which have to be located, for their effectiveness, between couple of points
 99 subjected to high relative displacements. The supplementary energy dissipation provided by
 100 such devices allows the reduction of the drift ϑ and, as a consequence, the reduction of the
 101 structural damage occurring at the beam ends. Conversely, the substitution strategy (Fig. 1c)
 102 allows the prevention of the structural damage, because all the dissipative zones are
 103 substituted by means of connections equipped with friction dampers. The expected drift
 104 demand does not reduce when comparison is made with traditional structures (Fig. 1a), but
 105 this drift leads to very limited structural damage in some joints components, because the
 106 rotation of the beam-to-column connections is accommodated by properly calibrating the

107 stroke of the friction dampers (Fig. 1c). The maximum rotation allowed is practically given by
108 the ratio between the damper stroke and the lever arm, i.e. its distance from the centre of
109 rotation CR. However, it is useful to note that the relative displacement occurring between the
110 ends of the friction damper ($\delta = \vartheta d_b$, being d_b the beam depth) is significantly less than the
111 one ($\delta = \vartheta h$, being h the interstorey height) occurring when the supplementary energy
112 dissipation strategy is applied (Fig. 1b). This is the main reason why cases a) and c) are
113 expected to provide similar drift demands. Finally, the best solution is obtained by combining
114 the substitution strategy with the supplementary energy dissipation strategy. Such combined
115 strategy (Fig. 1d) leads both to the reduction of the drift demands expected in case of
116 destructive seismic events and, in addition, to the prevention of significant damage in beam-
117 to-column connections. Obviously, the drift reduction is also an important benefit to reduce
118 damage to the building non-structural components.

119 Within the above framework, i.e. either substitution strategy or combined strategy, in this
120 paper a new beam-to-column connection equipped with friction dampers is investigated. In
121 particular, it is suggested to modify the classical detail of Double Split Tee Joints (DST) by
122 introducing a symmetrical friction damper at the level of the lower beam flange. With the
123 proposed connecting system, under bending actions, the joint is forced to rotate around the
124 upper T-stub, preventing slab damage, and the energy dissipation supply is provided by the
125 slippage of the lower beam flange on the friction pads which are made of steel plates coated
126 with thermally sprayed aluminium. In this way, provided that the steel components of the
127 connection are properly over-strengthened, the joint resistance and the rotation capacity can
128 be easily governed by calibrating the preload applied to the frictional interfaces and realizing
129 slotted holes whose length provides an adequate stroke for the dissipative device.

130 As the overall concept of equipping beam-to-column connections with friction dampers is not
131 new, it is important to underline the main differences with respect to similar connections
132 proposed by the New Zealand research group [39, 42, 44-45]. In particular, the main
133 differences regard the type of friction damper adopted and the material used for the friction
134 pads. In fact, the connection structural detail herein presented is based on the use of
135 symmetric friction damper while the sliding hinge joint proposed by Clifton et al. is based on
136 an asymmetric friction damper [39, 42]. The use of asymmetric friction dampers gives rise to
137 some yielding of the bolts which are subjected to bending moment, shear and axial force. Such
138 yielding is prevented when symmetric friction dampers are used like in the case of the beam-
139 to-column connections herein experimentally investigated. Moreover, the friction pads of the
140 connections herein investigated are made of steel plates coated by thermally sprayed

141 aluminium; conversely, other researchers have adopted brass or steel [38], bialloy steel
142 grade [39, 42, 44-45] or brake lining pads [37].

143 In order to validate the proposed beam-to-column connection system, an experimental
144 program has been carried out at the Materials and Structures Laboratory of Salerno
145 University and the results obtained are herein presented. In particular, the results of
146 preliminary tests aimed at characterizing the frictional properties of new pads coated by
147 thermally sprayed aluminium are described and, afterwards, the results of two tests on real-
148 scale external beam-to-column joints are presented. Furthermore, on the basis of the
149 component method, a design procedure -has been developed and adopted to design the
150 specimens The aim of the design procedure is to concentrate the energy dissipation in the
151 friction damper and to prevent the yielding of all the other joint components.

152

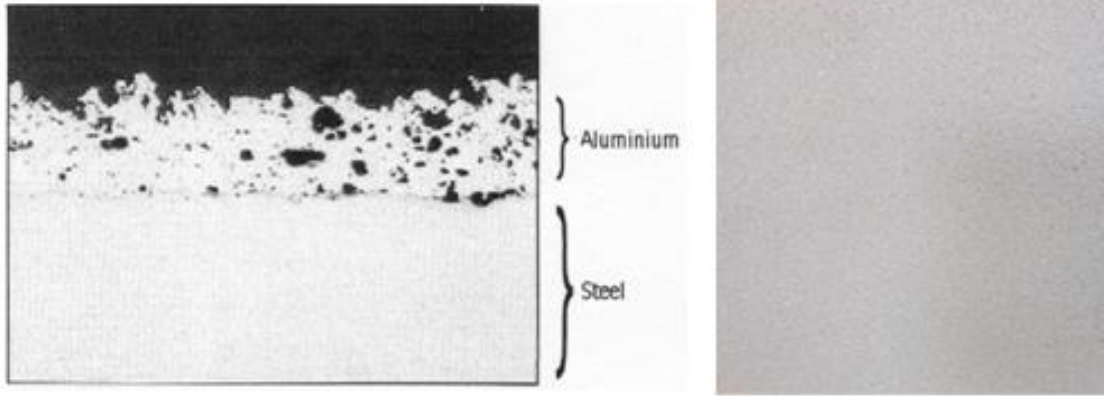
153 **2. EXPERIMENTAL ANALYSIS ON THERMALLY SPRAYED ALUMINUM INTERFACES**

154 The results here presented constitute the further development of work already carried out in
155 a previous experimental project dealing with the characterisation of frictional interfaces made
156 of brass, steel and three different types of rubber [46, 47]. The results herein presented are
157 referred to a new type of friction pad composed by an 8 mm S275JR steel plate (steel
158 hardness 211 HBW, sand blasted surface) coated with a thermally sprayed thin layer of
159 aluminium (Fig. 2). The use of thermally sprayed aluminium coatings can lead to high value of
160 the friction coefficient [49], thus allowing the reduction of the size of the friction damper.

161 Even though not exhaustively, thermal spray can be defined as the application of coatings by
162 means of special devices/systems through which melted or molten spray material is propelled
163 at high speed onto a cleaned and prepared surface of the component to be coated. The coating
164 feedstock material is melted by a heat source. This liquid or molten material is then propelled
165 by process gases and sprayed onto a base material, where it solidifies and forms a solid layer.

166 There are several different processes to apply a thermal sprayed coating. The process applied
167 for the friction pads herein investigated is the electric arc wire spray. Even though the main
168 field of application of sprayed aluminium is the prevention of corrosion phenomena, the high
169 values of the friction coefficient obtained and the low cost of the raw material have already
170 suggested its use for friction pads in damping technology [48, 49].

171



a) Cross section of the coating

b) Plan view of the surface

Figure 2: Cross-section of the coating and texture of the tested materials

172

173

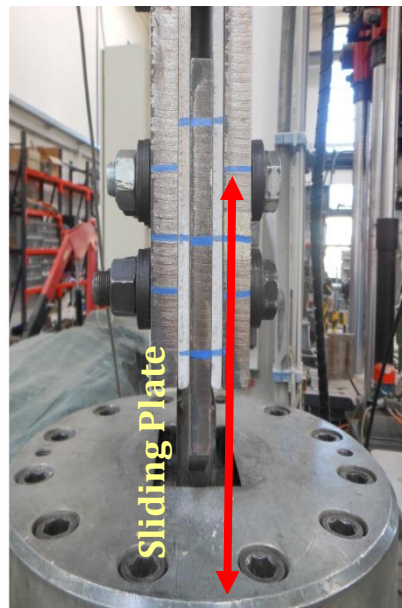
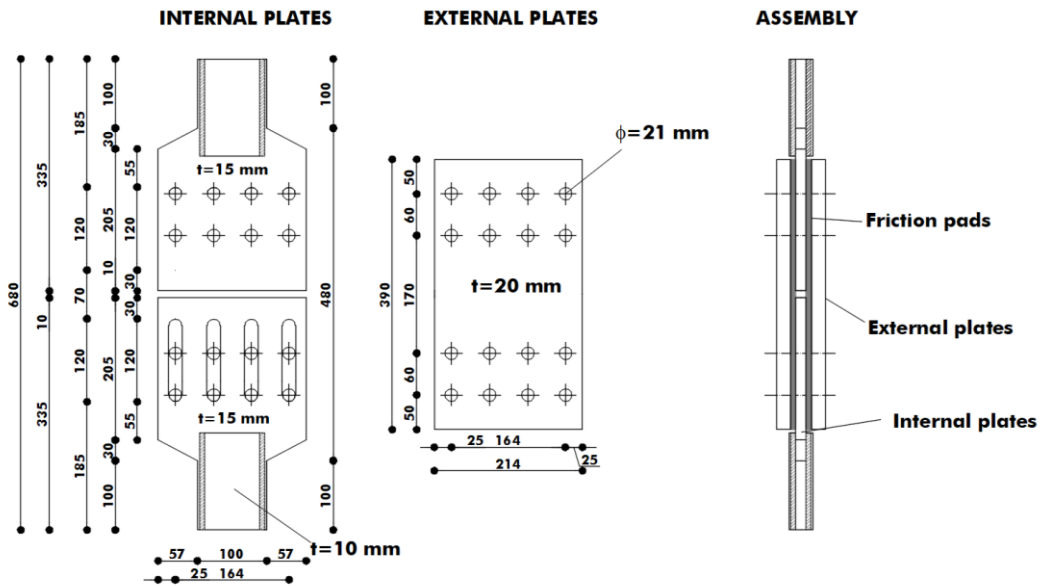


Figure 3: Geometry of specimens and testing equipment

174

175 In order to evaluate the friction coefficient of interfaces made of steel plates sliding on
176 thermally sprayed aluminium such as those adopted in the design of the proposed joint, a sub-
177 assemblage composed by a stack of S275JR steel plates has been employed. The device has
178 been designed to allow the slippage of one of the inner steel plates on the interposed material.
179 To this scope, such plate is realised with slotted holes, while the other inner and the two outer
180 plates are realised with circular holes (Fig. 3). The clamping force is applied to the friction pad
181 by means of a maximum number of 8 high strength pre-loadable M20 bolts of 10.9 class [16,
182 50,51] and, in order to reduce preloading losses during the test, cone annular disc springs
183 have been used in substitution of the classical circular flat washers [46, 47]. The disc springs
184 adopted conform to standard DIN 6796. The tests have been carried out by means of a
185 universal testing machine Schenck Hydropuls S56 (Fig. 3). In order to measure the axial
186 displacements the testing device is equipped with an LVDT, while the tension/compression
187 loads are measured by means of a load cell. The cyclic tests have been carried out under
188 displacement control for different amplitudes at a frequency equal to 0.25 Hz. This value has
189 been selected to be compatible with the capabilities of the testing equipment. Even though
190 this frequency does not correspond to the values occurring under actual seismic events, it
191 seems from the available technical literature that the influence of the velocity is not
192 particularly significant. In fact, the sliding force versus velocity relationship can be modelled
193 by means of a power expression where the exponent is close to zero [60].

194 The experimental analysis has been carried out in two phases. In the first phase, the influence
195 of the thickness of the coating layer on the value of the friction coefficient has been analysed
196 and the best value of the coating layer thickness has been selected. To this scope,
197 experimental tests have been carried out on specimens with different values of the thickness
198 of the sprayed aluminium coating. Successively, in the second phase, additional tests have
199 been carried out only on the selected interface to evaluate also the influence of the applied
200 pressure on the friction coefficient.

201 In particular, in the first phase, three different values of the coating thickness have been
202 considered ($50\ \mu\text{m}$, $150\ \mu\text{m}$ and $300\ \mu\text{m}$) by adopting for each one, two different loading
203 sequences as reported in Table 1. The torque has been assumed equal to 200 Nm and it has
204 been applied by means of a calibrated torque wrench, in order to achieve the desired bolt
205 preloading as described in Section 2.1. In the second phase, other two tests have been
206 performed only on the interface with coating thickness equal to $300\ \mu\text{m}$ considering other two
207 values of the tightening torque equal to $300\ \text{Nm}$ and $400\ \text{Nm}$. The tightening was applied
208 consistently with the European practice choosing among the possible available procedures

209 (torque, combined, HRC or DTI) the torque method, which is the only one that allows to
 210 tighten the bolts at values of the clamping force which are lower than the proof preload
 211 corresponding to the 70% of the bolt nominal resistance. In fact, while with the combined
 212 method, HRC bolts and DTI washers it is possible to control only that the proof preload is
 213 achieved, with the torque method intermediate values of the clamping force can be applied
 214 not losing accuracy. This is due, as explained in higher detail in Section 2.1, to the linear
 215 relationship that exists between torque and clamping force. More details on the accuracy of
 216 the tightening procedure when applied to friction dampers are given in [61].

217 **Table 1:** Summary of the tests carried out in the experimental programme

Coating Thickness	Number of tightened bolts	Bolt Torque	Number of Cycles of the loading sequence	Amplitude
50 μm	4	200 Nm	10	+/-15 mm
	8		45	
150 μm	4	200 Nm	10	+/- 15 mm
	8		45	
300 μm	4	200 Nm	10	+/- 15 mm
	8	200 Nm	20	
	4	300 Nm	10	
	4	400 Nm	10	

218 **2.1 TESTS ON THE COMPONENT**

219 The main goals of the experimental campaign are, on one hand, the evaluation of the friction
 220 coefficient for different values of the normal force acting on the sliding interface and, on the
 221 other hand, the assessment of the cyclic response in terms of stability of the cycles obtained
 222 and energy dissipation capacity. In the following the test results are discussed reporting the
 223 values obtained for the friction coefficient, determined as:

$$\mu = \frac{F}{n_s n_b N_b} \quad (1)$$

224 where n_s is the number of surfaces in contact, n_b is the number of bolts, N_b is the bolt
 225 preloading force and F is the sliding force. In particular, the bolt preloading force N_b is
 226 determined starting from the knowledge of the tightening torque by means of the following
 227 expression:

$$N_b = \frac{T_b}{k d_b} \quad (2)$$

228 where T_b is the value of the tightening torque, k is a factor accounting for the friction arising
 229 between the bolt nut and the plate and between the threads of the bolt shank and nut and d_b is
 230 the bolt nominal diameter. In agreement with [54] the value of k has been assumed equal to
 231 0.20.

232 Even though it is common practice to derive the friction coefficient of such devices by means
 233 of Eq. (1), it is useful to note that, according to EN 1993-1-8 [18], the design slip resistance has
 234 to be computed as:

$$F_{s,Rd} = \frac{k_s n_s n_b N_b}{\gamma_{M3}} \quad (3)$$

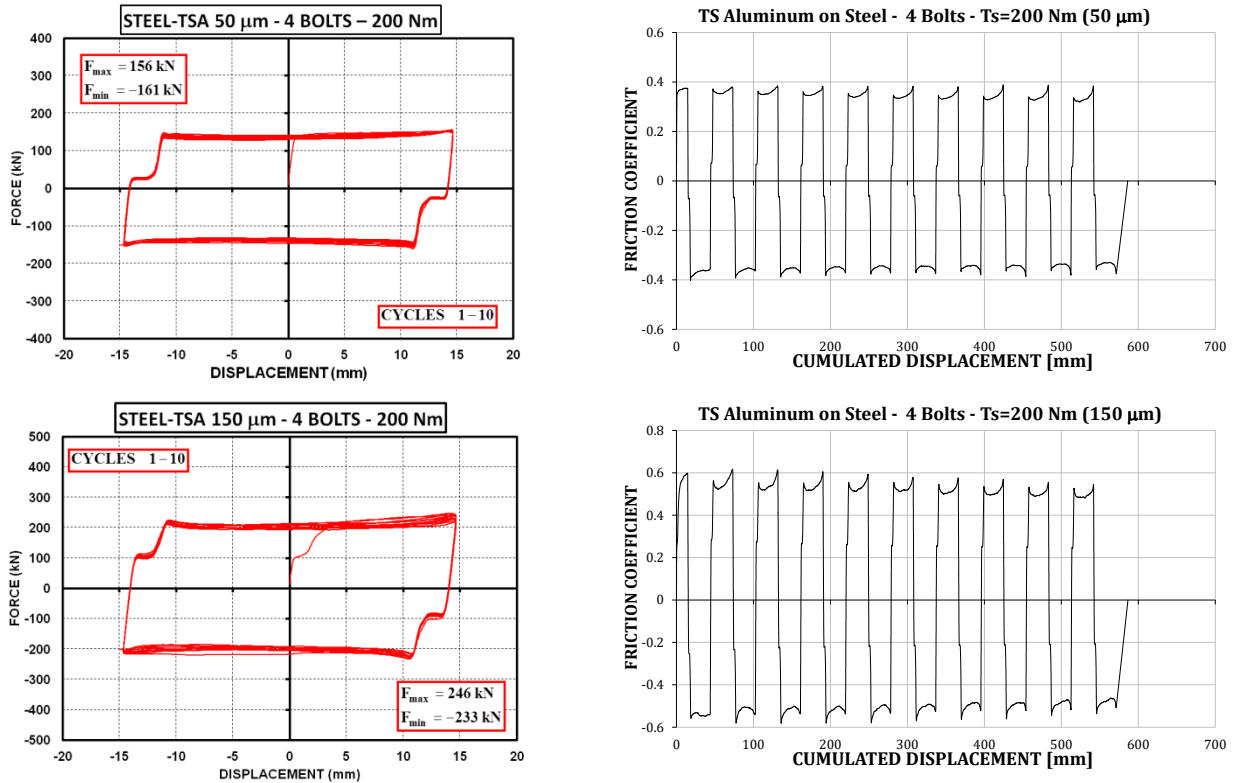
235 where γ_{M3} is the partial safety factor, to be assumed equal to 1.25 for ultimate limit states and
 236 equal to 1.10 for serviceability limit states, and k_s is a coefficient accounting for the hole
 237 typology. In particular, in case of long slotted holes (i.e. with clearance on the length at least
 238 equal to $1.5d$ [55]) with the axes of the slot parallel to the direction of load transfer, the value
 239 $k_s=0.63$ is suggested.

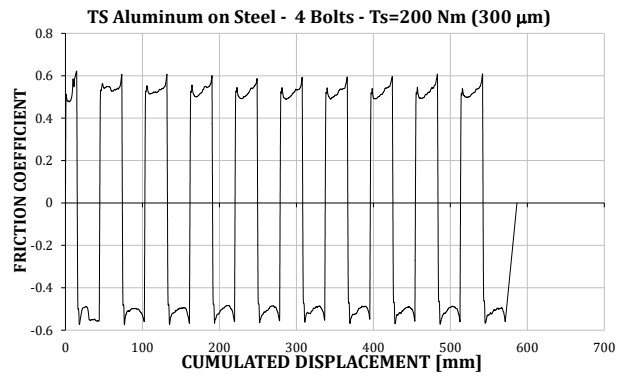
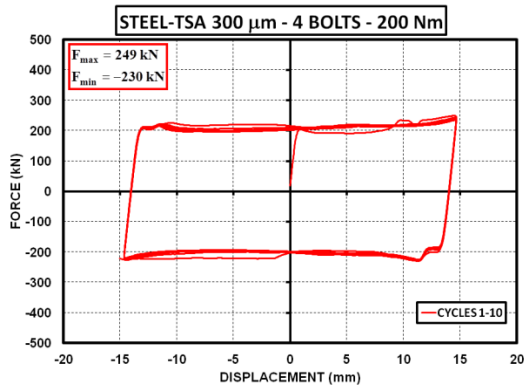
240

241 2.1.1 Tests with variable thickness of the coating layer

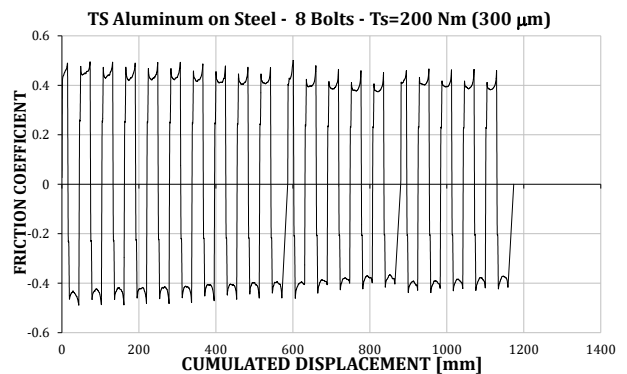
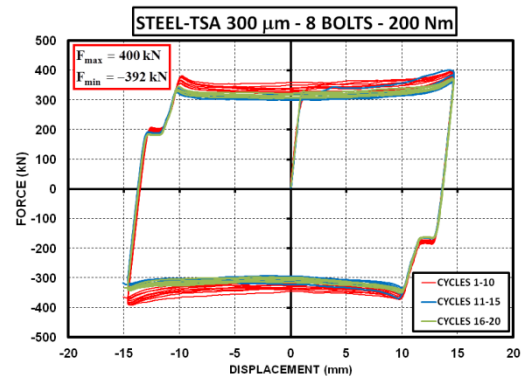
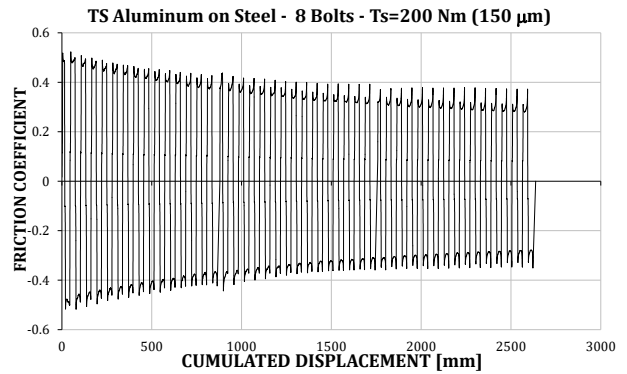
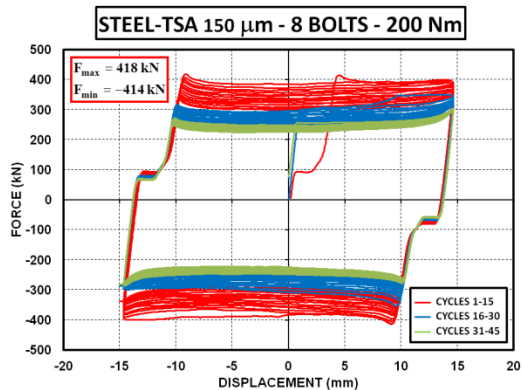
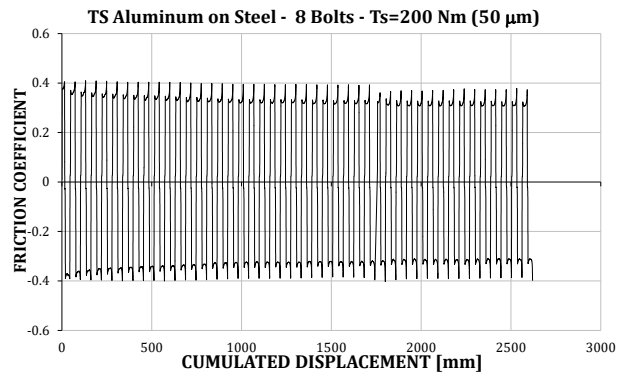
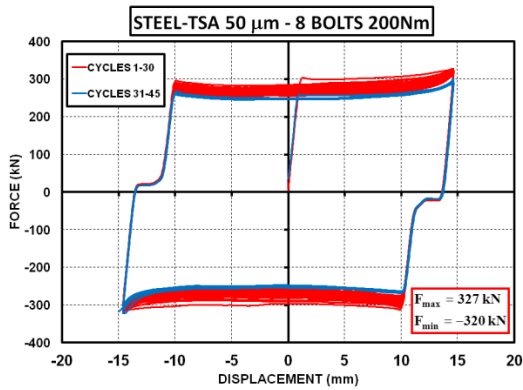
242 In order to evaluate the slip resistance of aluminium sprayed surfaces, sliding on steel,
 243 characterized by a different value of the coating thickness, different tests have been carried
 244 out. As a synthesis of the results, some of the tests and the values of the friction coefficient
 245 versus the cumulated displacement are delivered in Fig. 4, with reference to the group of
 246 specimens of the 2nd loading sequence. The results obtained are summarized in Table 2.

1st Loading Sequence





2nd Loading Sequence



247 **Figure 4:** Results obtained with coatings having different thickness

248 The results of the tests point out that the behaviour of all the interfaces is quite stable. All the
 249 interfaces exhibited a high initial stiffness and, after reaching the sliding force, began to slide

250 with a force similar to the initial one, evidencing that there is not a significant difference
251 between the static and kinetic coefficient of friction.

252 It useful to note that the displacements given in Fig. 4 are total displacements including also
253 the elastic contribution due to the axial stiffness of the plate elements constituting the
254 specimens.

255 In addition, after the first cycle, all the subsequent cycles reached a value of the maximum
256 force slightly lower than the initial one, evidencing the role played by the wearing of the
257 friction material of the coated surface (Fig. 5). However, regarding the degradation of the slip
258 resistance occurring as far as the cumulated displacement increases, it is useful to point out
259 that, in case of destructive seismic events, the friction dampers equipping beam-to-column
260 connections are expected to be subjected to cumulated displacement of about 250 mm [56],
261 so that the degradation pointed out in Fig. 4 can occur only in case of repeated earthquakes.

262 Analyzing the results summarized in Table 2, it is possible to observe that, considering all the
263 tested interfaces, the value of the friction coefficient ranges in between 0.37 and 0.59,
264 revealing that thermally sprayed aluminium is able to provide a value of the coefficient of
265 friction higher than the metallic and rubber interfaces tested in past experimental
266 investigations [46]. In particular, the highest value of the friction coefficient was obtained
267 with the thickness of 150 μm and the lowest with the thickness of 50 μm .

268 In addition, the reported tests show that the degradation of the sliding force significantly
269 depends on the thickness of aluminium coating. In fact, considering the first loading sequence
270 (Table 2), in case of 50 μm and 300 μm thickness, the degradation of the sliding force is very
271 low and the ratio between the initial and final friction coefficient is equal to 1.12 and 1.02
272 respectively. In the first case, probably the result is due to the lower sliding force that
273 provided a limited consumption of the friction pad. Conversely, a higher degradation was
274 shown by the 150 μm interface, whose initial/final sliding force ratio was equal to 1.22.
275 Therefore, analyzing the results on these tests, for the subsequent phase of the experimental
276 work, only the coating with thickness of 300 μm has been considered. In fact, as a result of the
277 first phase tests, this thickness of the coating layer is believed to provide a good compromise
278 between the initial value of friction coefficient and degradation of the sliding force during a
279 cyclic loading history.

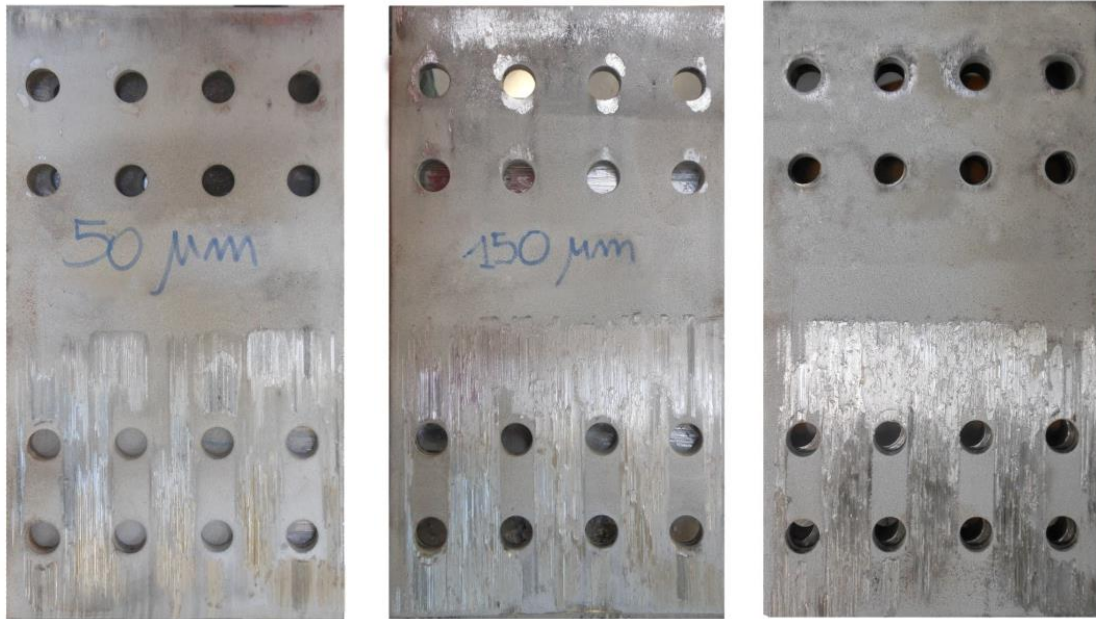


Figure 5: Appearance of surface of friction pads after testing

Table 2: Friction coefficients obtained for different coating thickness

Thickness of the coating	1 st loading sequence		2 nd loading sequence	
	Initial	Final	Initial	Final
50 μm	0.37	0.33	0.37	0.31
150 μm	0.59	0.48	0.52	0.29
300 μm	0.52	0.51	0.45	0.37

280
281
282
283
284
285
286
287
288
289
290
291
292
293
294
295
296
297
298
299

Regarding the values of the friction coefficient obtained, it is useful to note that the values given in Table 2 could seem comparable with those which can be obtained by means of shot blasted steel, so that the incentive in using sprayed aluminium could seem not much. As an example, a recent experimental program dealing with the design of slip resistance lap joints [57] has shown, in case of normal holes, a friction coefficient equal to 0.56 in case of joints made of S275 steel whose surface is blasted with shot steel to Sa 2^{1/2} and equal to 0.52 in case of joints made of S275 steel whose surface is blasted with shot steel to Sa 3 and spray-metalized with 75 μm zinc. However, it has to be considered that the values given in Table 2 are obtained for long slotted holes, so that they are also the result of a smaller contact area leading to higher local pressures. The influence of the hole typology is accounted for by means of the coefficient k_s in Eq. (3) which, according to Eurocode 3, is equal to 0.63 aiming to provide a safe side value of the slip resistance. According to [58], such influence is about 30% in case of long slotted holes, so that the value 0.59 obtained in case of 150 μm coating thickness is equivalent to a value of about 0.77 for normal holes. This consideration points out the advantage which can be obtained by means of thermally sprayed aluminium.

300 Moreover, it is useful to note that values of the friction coefficient higher than those obtained
 301 in the experimental tests herein presented have been obtained by other researchers [48]. This
 302 difference can be attributed to the differences in the preliminary treatments applied before
 303 thermal spraying and/or to the main setting parameters of the machine employed to apply
 304 the coatings, i.e. the amperage, voltage and pressure of the air, which have to be changed
 305 according to the melting temperature of the materials applied.

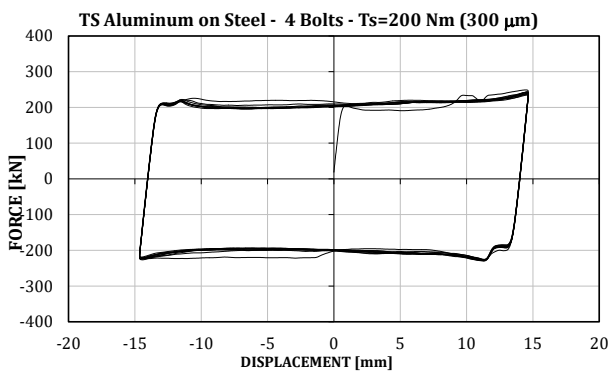
306

307 *2.1.2 Tests with variable pressure*

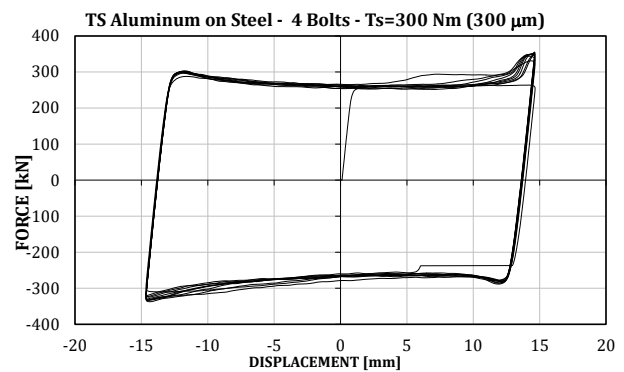
308

309 As aforesaid, in order to evaluate the influence of the tightening pressure on the value of the
 310 slip resistance, additional tests have been carried on further specimens having the selected
 311 coating thickness. In particular, three different values of the tightening torque have been
 312 considered and only one loading sequence of ten cycles with amplitude of +/- 15 mm has been
 313 adopted. The behaviour exhibited by such specimens is reported in Fig. 6. It evidences a
 314 response very similar to that reported in previous tests, but reveals that the value of the initial
 315 coefficient of friction, for this interface, is also affected by the pressure applied on the
 316 interface. In fact, as it is possible to observe, as far as the value of the tightening torque
 317 increases, the initial friction coefficient decreases (Fig. 7).

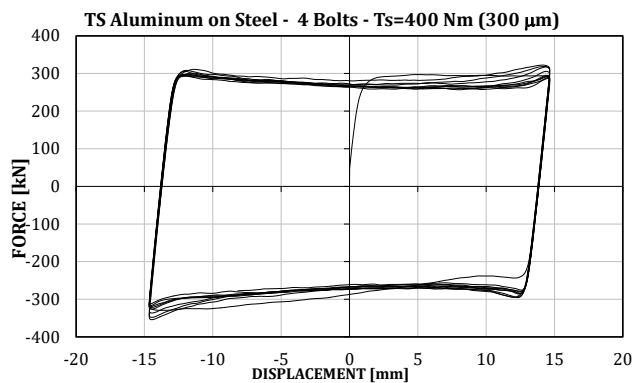
318



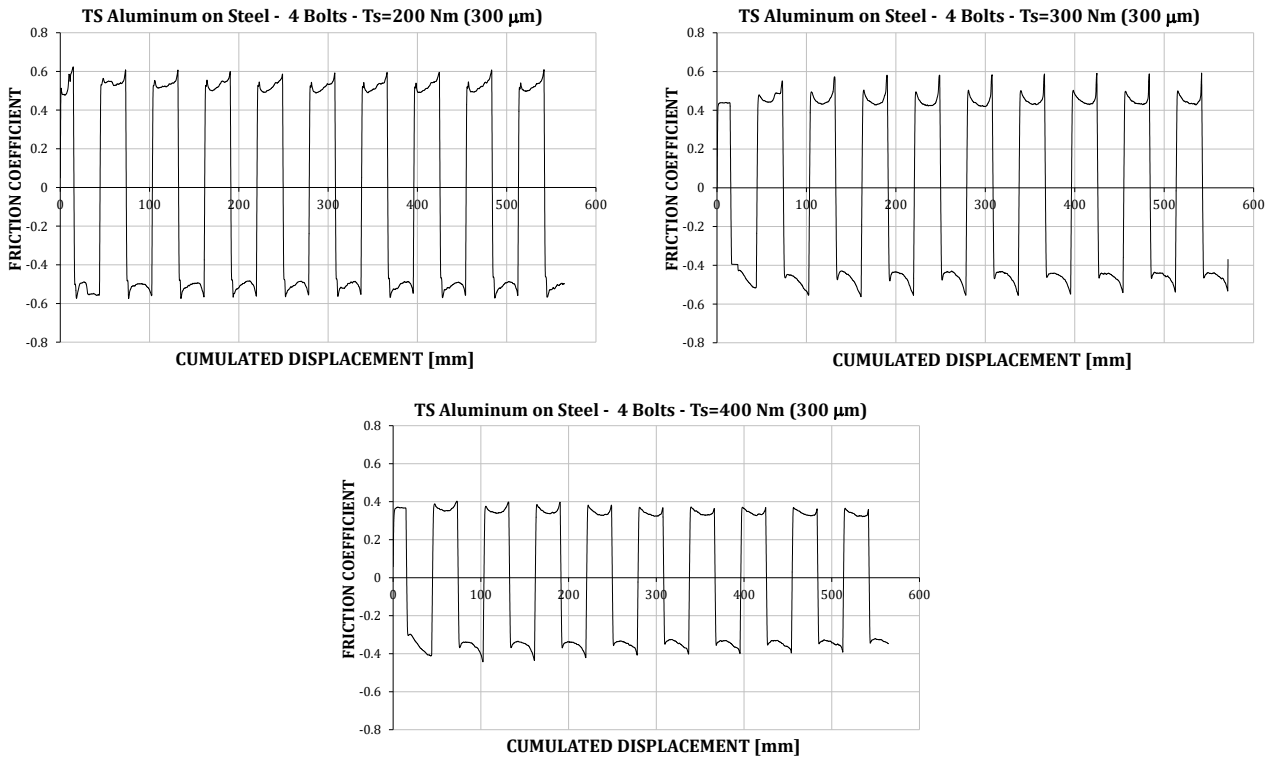
(Ts=200Nm)



(Ts=300Nm)



(Ts=400Nm)

Figure 6: *Cyclic response for different values of the applied tightening torque*

320

Figure 7: *Friction coefficient vs. cumulated displacement for different tightening levels*

321

322 Therefore, in order to develop a mechanical model to design beam-to-column connections
 323 equipped with friction dampers with thermally sprayed aluminium pads, a relationship
 324 providing the initial friction coefficient as a function of the pressure applied at the interface
 325 has been derived. To this scope, the pressure applied at the interface has been estimated
 326 assuming that the normal force is transferred by the bolts to the plates spreading with a slope
 327 equal to 45°, obtaining the following equation which includes the influence of the long slotted
 328 hole (Fig. 8):

329

$$p = \frac{4N_b}{\pi \xi^2 d_b^2 \left(1 - 2 \frac{\arcsin(\eta/\xi)}{\pi} - \frac{\eta}{\pi \xi} \sqrt{1 - \left(\frac{\eta}{\xi}\right)^2} \right)^2} \quad (4)$$

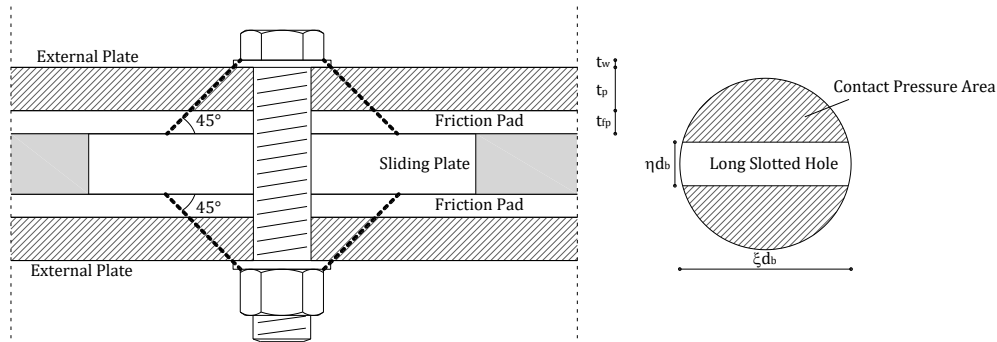
330

331 where ηd_b is the slot width and:

$$\xi = \frac{d_{bh} + 2(t_w + t_p + t_{fp})}{d_b} \quad (5)$$

332

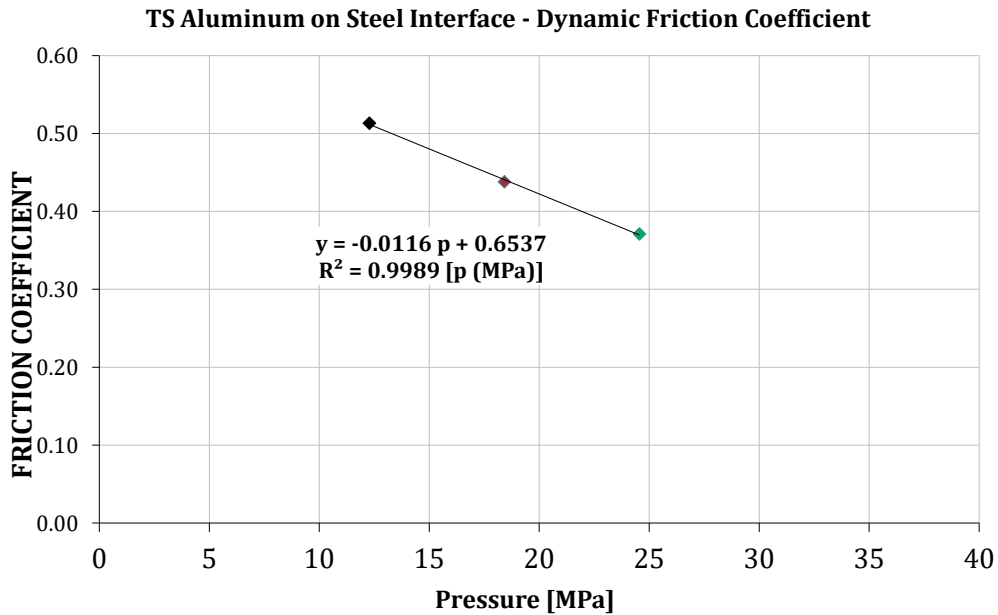
333 being d_b the bolt diameter, d_{bh} the bolt head diameter, t_w the washer thickness, t_p the outer
 334 plate thickness and t_{fp} the friction pad thickness.



335
 336 **Figure 8:** Assumed geometry of the contact pressure area

337 It is useful to note that the above relationships are valid provided that the distance between
 338 the slots and the bolt pitch is greater than ξd_b and, in addition, the distance between the slot
 339 and the plate edge is greater than $\xi d_b / 2$. When such conditions are not satisfied the
 340 interaction has to be accounted for. In Fig. 9 the result of the regression analysis of the
 341 experimental data is reported. **Nevertheless, being referred only to three experimental data,**
 342 **this regression has to be considered with some caution.**

343 The influence of the pressure on the friction coefficient is justified considering that all
 344 surfaces are rough on a microscopic scale and real contact is obtained over a small fraction of
 345 the apparent contact area. Friction is related to the real contact area and independent of the
 346 apparent contact area. Real contact area is affected by the applied pressure which, therefore,
 347 affects the resulting friction coefficient. In particular, the increase of the applied pressure
 348 tends, on one hand, to flatten the surface asperities, thus reducing the amount of friction due
 349 to the mechanism of asperity interlocking and, on the other hand, to increase the real contact
 350 area thus improving the adhesion mechanism. The prevailing between these two phenomena
 351 will govern the dependence of the friction coefficient on pressure and can be investigated by
 352 experimental results only.



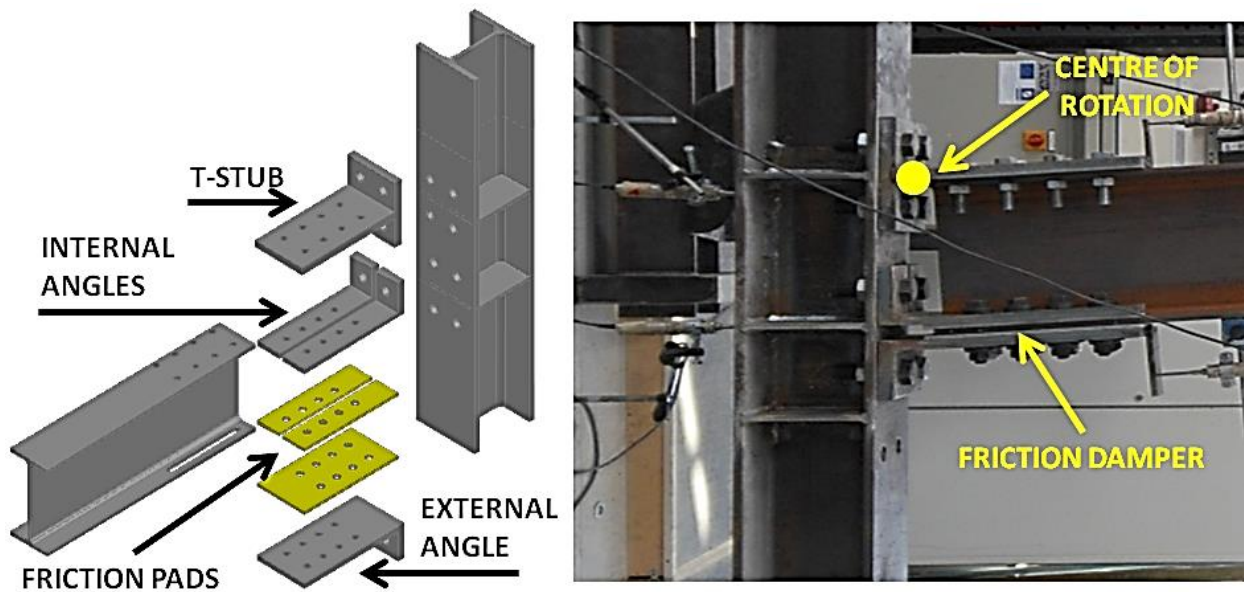
353
354 *Figure 9: Influence of the contact pressure on the friction coefficient*
355

356 **3 CONCEPT AND DESIGN OF TESTED SPECIMENS**

357 Starting from the above results, the design of dissipative connections equipped with friction
358 dampers was performed. The joint detail proposed in this paper is the modification of the
359 classical detail of a double split tee beam-to-column connection obtained by connecting the
360 beam bottom flange to the column flange by means of three steel angles, composed by
361 welding, and by interposing between them and the beam flange one or two friction pads (Fig.
362 10). In this way, the energy dissipation supply is provided by the friction damper, while all the
363 other elements of the connection and the beam are designed in order to be free from yielding.
364 Exception has to be made for the stem of T-stub and angles, close to the T-stub flange and
365 vertical angle leg respectively, which in order to accommodate the rotation are subjected to
366 minor yielding. This strategy, as already demonstrated in some preliminary studies on similar
367 prototypes, allows the development of beam-to-column connections with high energy
368 dissipation able to accommodate the required rotations without any significant damage [47].
369 The classical T-stub connection at the top flange level is aimed to fix the centre of rotation
370 with the goal of preventing the damage to the reinforced concrete slab, while the bottom
371 damper provides, thanks to its stroke, the required rotation capacity and the energy
372 dissipation.

373 A significant advantage of this joint configuration is that, by controlling the tightening torque
374 applied to the bolts, it is possible to calibrate magnitude of the sliding resistance of the friction
375 damper and, therefore, depending on the lever arm, the magnitude of the bending moment

376 transmitted to the column. It is useful to note that, in order to assure that the beam end
377 remains in elastic range, the bending sliding resistance of the connection has to be not greater
378 than the nominal bending resistance of the connected beam. However, in order to maximize
379 the exploitation of the beam under gravity loads and under the internal actions occurring
380 when the structure is subjected to horizontal forces corresponding to serviceability limit
381 states, such as wind actions or frequent seismic events having a low return period, the ratio
382 between the bending sliding resistance of the connection and the nominal bending resistance
383 of the connected beam has to be as close as possible to 1.0. In order to satisfy the above design
384 criterion and to maximize the exploitation of the connected beam, the use of a beam end
385 haunch to increase and calibrate the lever arm can also be suggested (Fig. 11). In such a way,
386 the beam section is fully exploited, but both the oversizing of the other joint components
387 (such as the panel zone usually requiring supplementary web plates, the beam end requiring
388 reinforcing ribs or cover plates, the increase of the bolt diameter, etc.) and the column
389 oversizing (because of beam-column hierarchy criterion) can be significantly limited and/or
390 controlled.



391
392 **Figure 10: Beam-to-column connection equipped with friction dampers**
393

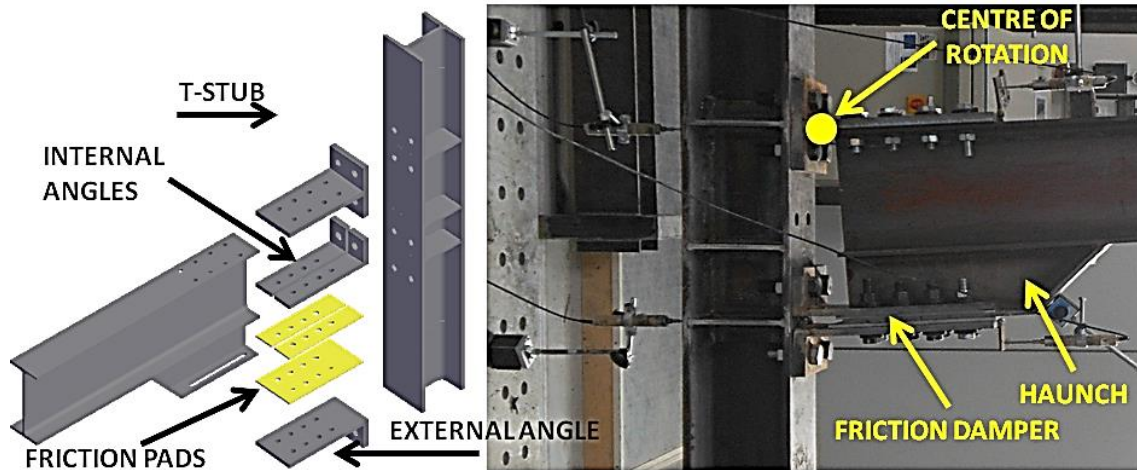


Figure 11: Beam-to-column connection equipped with friction dampers and additional haunch

394
395

396

397

398

399

400

Within the experimental activity described in this paper two different joints equipped with the friction damper previously tested under uniaxial loading conditions were tested under cyclic loading conditions. In particular, the two joints fasten an IPE270 beam to an HEB200 column, both of them made of S275 steel. They are identified as follows:

401

402

403

404

405

- **TSJ-SA300-320-CYC12:** it is a joint where the upper beam flange is connected to the column by means of a T-stub, while the lower beam flange is fastened to the column by means of a system of three angles (Fig. 10). Three steel plates with a 300 μm coating of thermally sprayed aluminium are located in between the beam flange and the angles in order to realize the friction damper;

406

407

408

409

- **TSJ-H-SA300-260-CYC13:** it is a joint with a detail very similar to the previous one where, in order to increase the lever arm, the friction damper is applied by means of an additional haunch which is welded to the beam. This allows the reduction of the tightening torque and/or of the number of bolts (Fig. 11).

410

411

412

413

414

415

416

417

418

419

Starting from the values of the friction coefficients derived in previous section, the design of the dissipative connections equipped with friction pads was performed. Within the framework of the component method, the following components have to be designed: the shear panel, the column web panels in tension and compression, the T-stub/angles and the friction damper. In order to obtain a joint where the only component providing energy dissipation is the friction damper, the steel parts have to possess sufficient overstrength with respect to the maximum force that the friction damper is able to transmit. According to this hierarchy, the geometry of all the elements composing the joint was defined by exploiting the formulations provided by literature models or by means of the formulations given in Eurocode 3 [17].

420 Specimen TSJ-SA300-320-CYC12 was designed to develop a bending moment evaluated at the
421 level of the column face equal to the beam nominal plastic resistance (133 kNm). It means that
422 the joint was designed to assure that the beam end remains in elastic range. In fact,
423 considering that the friction damper is characterized by a rigid-plastic response, imposing
424 that the slip resistance of the damper occurs at the attainment of a bending moment equal to
425 the characteristic flexural resistance of the beam, assures that the connected member remains
426 elastic. A similar criterion has been adopted for specimen TSJ-H-SA300-260-CYC13
427 accounting, however, for the possibility to increase the slip resistance of the connection
428 beyond the nominal resistance of the beam evaluated at the column face. In fact, in this case, it
429 is possible to account for the increase of resistance of the beam in the haunched part
430 increasing, consequently, the slip resistance of the damper. Therefore, this joint has been
431 designed to develop a bending moment equal to 1.4 times the beam nominal resistance,
432 namely 187 kNm. Taking into account that the beam length (i.e. the distance between the
433 actuator and the column face) is equal to 1460 mm and that the un-strengthened segment of
434 the beam is equal to 885 mm, when the design bending moment at the column face is achieved
435 (187 kNm), the bending moment acting at the end of the haunch is equal to
436 $187 \times 885 / 1460 \cong 113$ kNm (which is about 0.85 times the beam nominal resistance). It means
437 that also for this specimen, when slippage occurs, the bending moment in the un-strengthened
438 portion of the beam is lower than the beam nominal resistance, assuring that it remains
439 elastic. These reference values of the flexural resistance were used to define the tightening
440 torque of the bolts of the friction damper accounting for the friction coefficient values
441 previously reported.

442 All the remaining joint components have been designed with an appropriate overstrength. In
443 particular, the column shear panel has been reinforced with a couple of 10 mm
444 supplementary plates welded on the column web, while the panels in tension and
445 compression have been stiffened with a couple of continuity plates with a thickness equal to
446 the beam flange thickness. However, in order to obtain structural details which are more cost
447 effective the possibility to omit these strengthening elements can be evaluated. In addition,
448 the upper T-stub and the lower angles have been designed in order to remain in elastic range
449 under a force level corresponding to the friction damper design force.

450 Dealing with the friction damper, the parameters to be controlled in the design are the length
451 of the slots made on the beam flange or on the haunch (which allow the slip of the beam flange
452 on the friction pad) and the tightening torque to be applied to the bolts which are used to
453 preload the friction pads. In particular, the first parameter governs the rotational capacity of

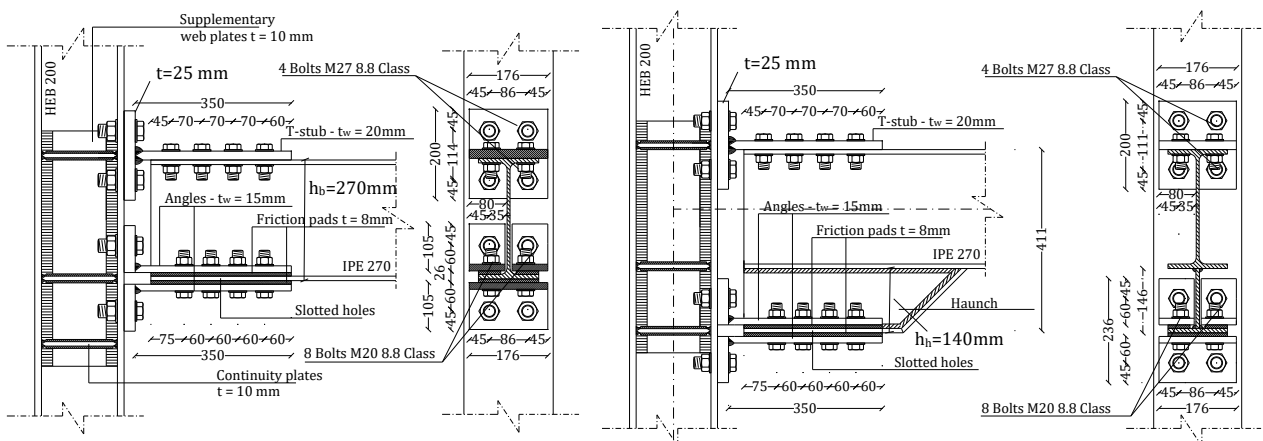
454 the connection and, as a consequence, it can be selected starting from the expected value of
 455 the joint rotation (ϕ) under the most severe design earthquake, by using the following
 456 equation:

$$L_{slot} = (n_{br} - 1)p + d_b + 2\phi z \quad (6)$$

457 where d_b is the bolts diameter, n_{br} is the number of bolt rows used to fasten the stem of the
 458 angles to the beam bottom flange, p is the bolt pitch and z is the lever arm. For the tested
 459 specimens $d_b=20$ mm, $n_{br}=4$, $p=60$ mm and $z = 265$ mm for specimen TSJ-SA300-320-CYC12
 460 and $z = 411$ mm for specimen TSJ-H-SA300-260-CYC13, respectively. Therefore, by assuming
 461 $\phi=0.08$ rad, according to this criterion a length of the slot equal to 270 mm has been chosen
 462 for the two joints. The clear gap between the beam edge and the inside of the flange of the Tee
 463 section has been assumed equal to about two times the thickness of T-stub stem to allow the
 464 local yielding required to accommodate the beam rotation.

465 The second parameter governs the magnitude of the bending moment that the joint is able to
 466 withstand before the slippage of the friction damper occurs. In particular, the design force of
 467 the friction damper can be easily defined as the design bending moment divided by the lever
 468 arm. The design friction resistance of the damper device is equal to $133/0.265 \cong 502$ kN in
 469 case of specimen TSJ-SA300-320-CYC12 and equal to $187/0.411 \cong 455$ kN in case of specimen
 470 TSJ-H-SA300-260-CYC 13. Starting from the knowledge of the friction damper design force,
 471 exploiting Equations (1) and (2) and the relationship between the friction coefficient and the
 472 pressure applied at the interface (Fig. 9), it is possible to determine the value of the tightening
 473 torque to be applied, equal to 320 Nm and 260 Nm for the two tested specimens. The details
 474 of the specimens are delivered in Fig. 12.

475



476

477

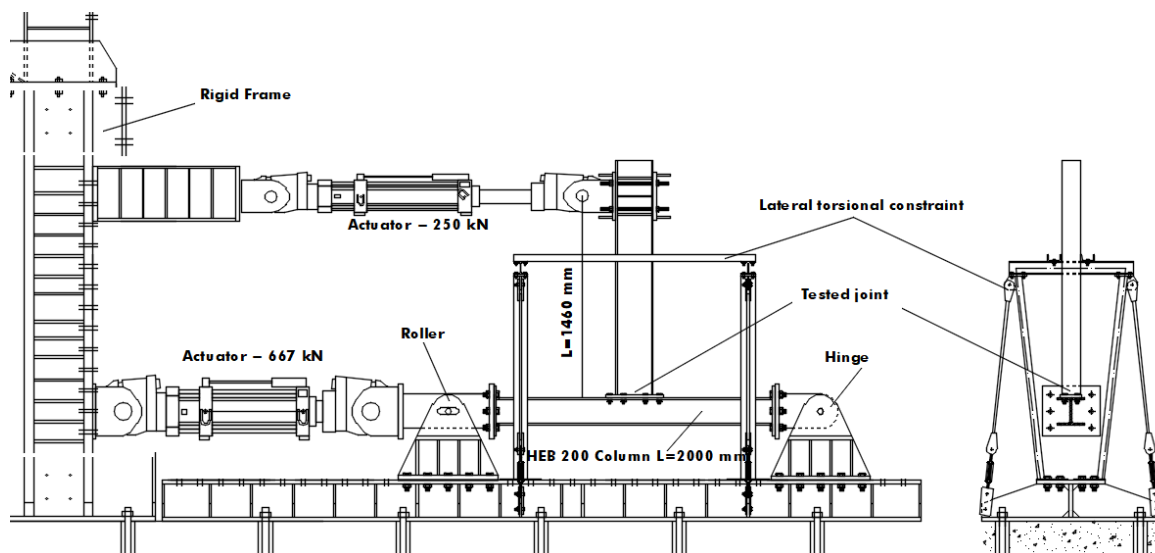
478

Figure 12: Details of the tested specimens. Left: TSJ-SA300-320-CYC12; Right: TSJ-SA300-260-CYC13

479

480 4 EXPERIMENTAL LAYOUT

481 The experimental tests were carried out at Materials and Structures Laboratory of Salerno
482 University. Two steel hinges, designed to resist shear actions up to 2000 kN and bolted to the
483 strong floor base beam, were adopted to connect the specimens to the reacting system. The
484 specimens were assembled with the column (HEB 200) in horizontal position, connected to
485 the hinges, and the beam (IPE 270) in vertical position (Fig. 13). The loads were applied by
486 means of two different hydraulic actuators. The first one used to apply, under force control, an
487 axial load in the column equal to 30% of the squash load. The second actuator to apply, under
488 displacement control, the desired displacement history at the beam end. In order to avoid the
489 lateral-torsional buckling of the beam, an horizontal transversal frame was conceived to work
490 as a guide which restrains the lateral displacement of the beam. The loading history was
491 defined in terms of drift angle, according to the testing protocol provided by AISC, 2005 [59].



492

493

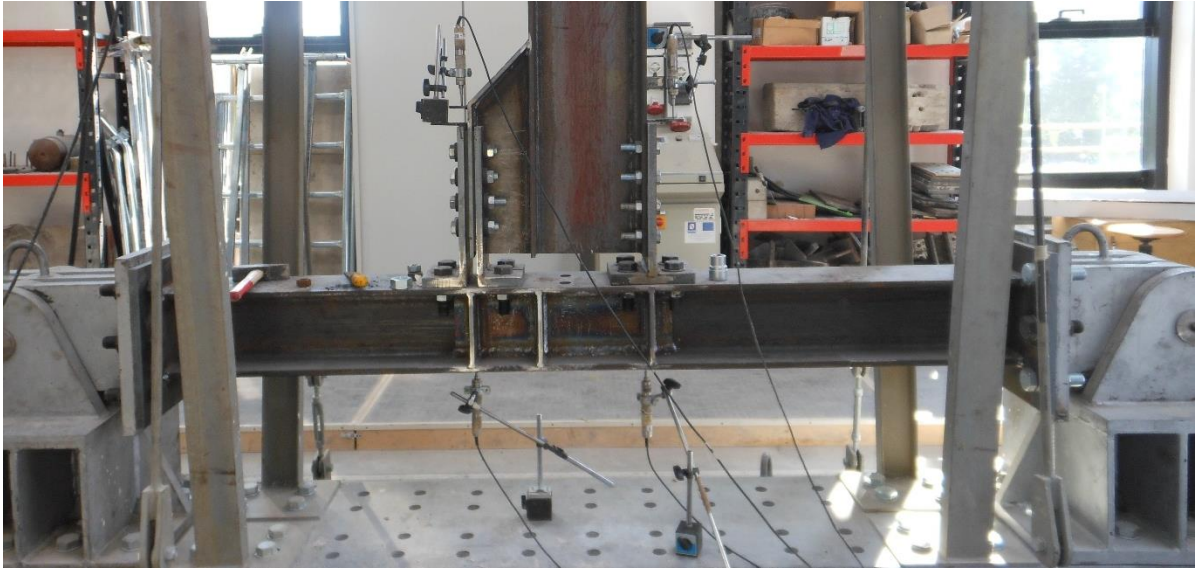
Figure 13: Experimental layout for tests on joints

494 During the tests the displacement history imposed by the top actuator and the displacements
495 of the different joint components were acquired. In particular, in each test, four LVDT were
496 used to measure the local displacement of the friction damper, the rotation of the panel zone
497 and to control that the axial displacements exhibited by the fixed T-stub were negligible (Fig.
498 14).

499 Aiming at the evaluation of the beam end displacements due to the beam-to-column joint
500 rotation only, the top displacements of the cantilever beam measured by means of the LVDT
501 equipping the actuator were corrected by subtracting the elastic contribution due to the beam
502 and column flexural deformability according to the following relationship:

$$\delta_j = \delta_{MTS} - \frac{FL_b^3}{3EI_b} - \frac{FL_c L_b^2}{12EI_c} \left[\left(\frac{L_c}{L_c + 2a} \right)^2 + \frac{6a}{L_c + 2a} \right] \quad (7)$$

503



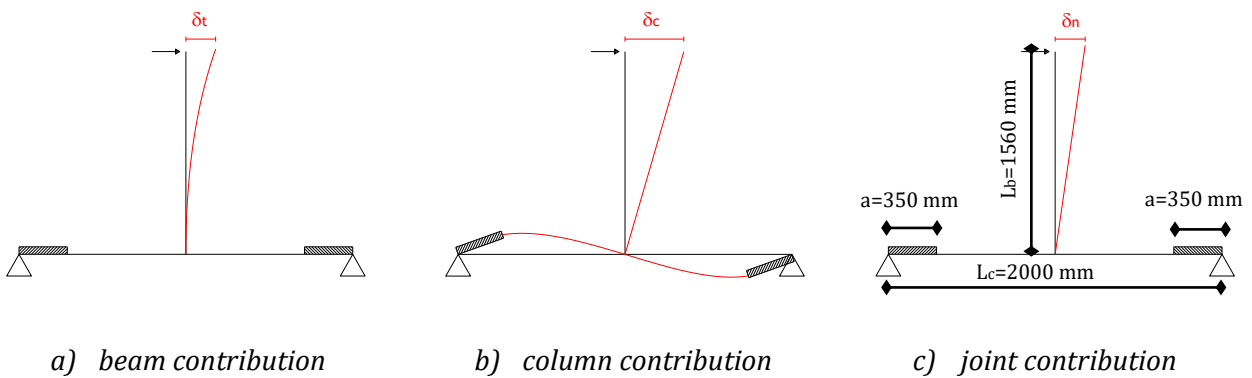
504

505

Figure 14: Position of LVDTs used to measure the local displacements

506

507 where δ_{MTS} is the overall top horizontal displacement evaluated at the level of MTS actuator, I_b
 508 and I_c are the beam and column inertia moments, L_c is the column length, L_b is the beam length
 509 and a is the length of the rigid parts, due to the steel hinges (Fig. 15).



510

511

Figure 15: Scheme for evaluating the joint contributions to the overall top displacement

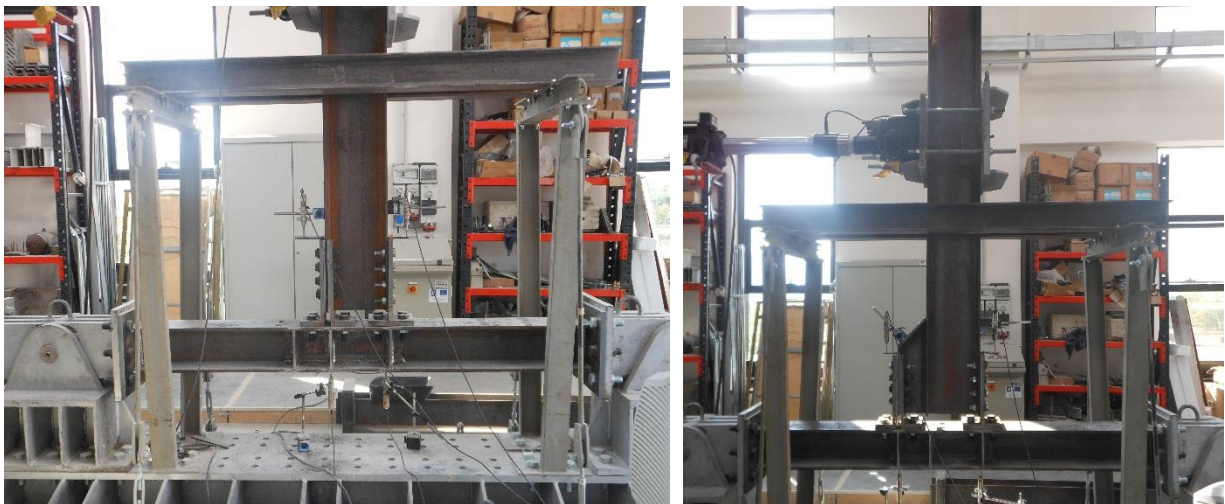
512

513 The identification label of the tests refers to the following issues: 1- Joint typology, i.e. Tee
 514 Stub Joint (TSJ) or Tee Stub Joint with haunch (TSJ-H) / 2 - Friction interface, i.e. SA300
 515 (Sprayed Aluminium with 300 μ m coating) / 3 - Tightening torque of the bolts in Nm / 4 -
 516 Progressive number of cyclic tests, i.e. CYCXX.

517

518 **5 CYCLIC BEHAVIOR OF SPECIMENS**

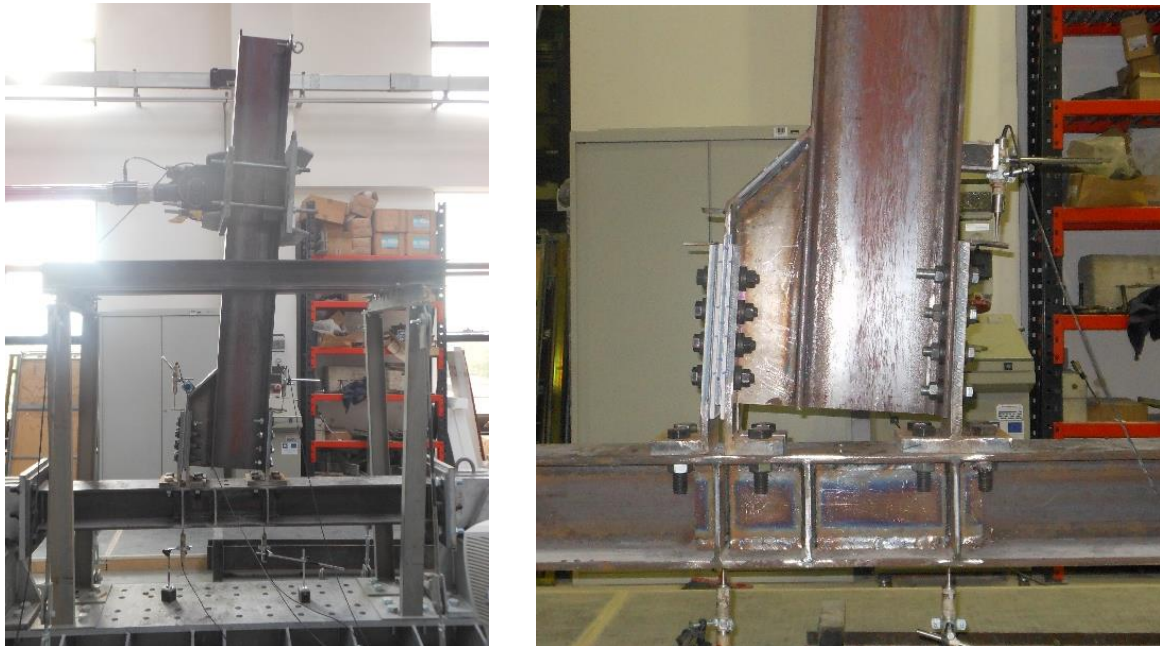
519 As aforesaid, the two joints (Fig. 16) were tested under cyclic loading conditions following the
520 drift history suggested by the AISC loading protocol. As expected, on the basis of the design
521 criteria adopted, in all the experimental tests there has not been any significant damage of the
522 joint components, but only the wearing of the friction pads. Therefore, a very important
523 outcome of the experimental program is the verification that this connection typology can be
524 subjected to repeated cyclic rotation histories, i.e. to repeated earthquakes, by only
525 substituting the friction pads, if needed, and by tightening again the bolts to reach the desired
526 preloading level. In addition, the rotation capacity can be easily calibrated by simply
527 governing the length of the slotted holes. In fact, in all the tests the rotation demand applied to
528 the joint has been completely due to the slippage of the friction damper located at the bottom
529 beam flange. The experimental results are in line with the outcomes of the tests on the friction
530 interfaces pointing out that, as expected, the cyclic behaviour of the joint is mainly governed
531 by the cyclic behaviour of the weakest joint component, i.e. the friction damper.



532
533 **Figure 16: Specimens before testing**

534 In fact, in both tests the response has been very similar to that exhibited during the uniaxial
535 tests on the interface. At low force values the joints exhibited an elastic behaviour
536 characterized by a high initial stiffness. In particular, in case of joint TS-H-SA300-260-CYC13
537 the initial stiffness was sensibly higher due to the increased lever arm provided by the
538 additional haunch. When the force applied at the end of the cantilever beam reached a value
539 approximately equal to the design bending moment divided by the beam length, the slippage
540 of the friction dampers started (Figs. 17-18). After the first slippage, the joints hysteretic
541 response was characterized for all the loading/unloading cycles approximately by a

542 parallelogram shape with a slight strength degradation as the number of the cycles of the
543 loading history increases (Fig. 19).
544 By the comparison with the results of the tests carried out on the friction dampers (i.e. the
545 component alone), it is worth noting that the main difference between the hysteresis cycles of
546 the friction DST joint and those observed during the uniaxial tension test is the asymmetric
547 response. This difference is mainly due to the role played by the beam rotation in the
548 kinematic mechanism. In fact, the beam rotation causes two effects that give rise to an
549 increase of the bending moment as far as the beam rotation increases. On one hand, there is
550 an increase of the local pressure on the friction pads due to the reaction force provided by the
551 stem of the fixed T-stub at the top beam flange level and by the stems of the angles at the
552 bottom flange level, that behave in a way similar to a pocket foundation. Because of this
553 pocket foundation effect, the increase of the pressure on the friction pads depends on the
554 direction of the horizontal displacement of the cantilever. **Therefore, the asymmetry of the**
555 **cyclic response is due to the reduction of the friction coefficient when the pressure on the**
556 **friction pads increases. Additionally, when the dampers are in tension a deformation of the**
557 **steel angles occurs, probably providing a reduction of the bolt forces due to the opening of a**
558 **small gap in the web plates.** On the other hand, minor yielding of the tee stems at the stem-to-
559 flange connection of top T-stub and bottom angles contributes to the total bending resistance
560 providing a slight hardening behaviour as experimentally observed (Fig. 19).



561
562

Figure 17: Sliding motion of the friction damper

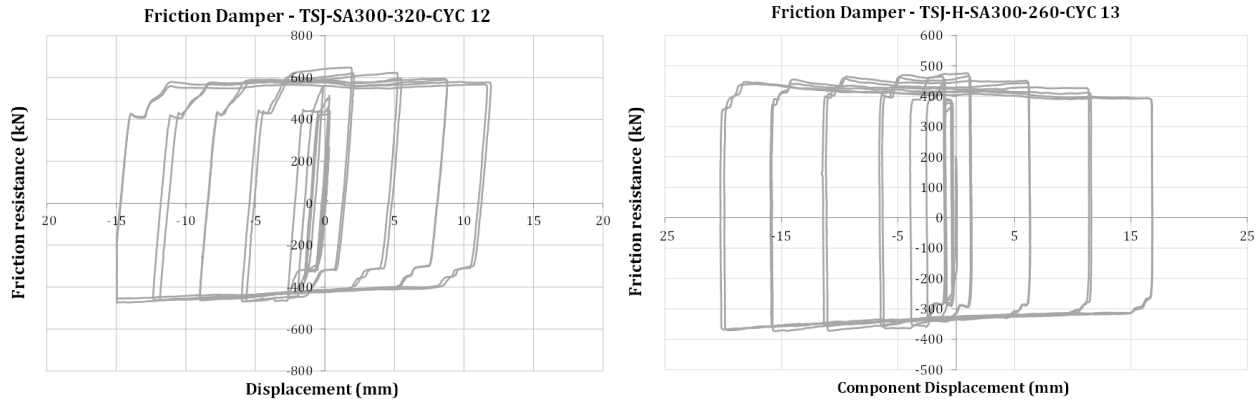
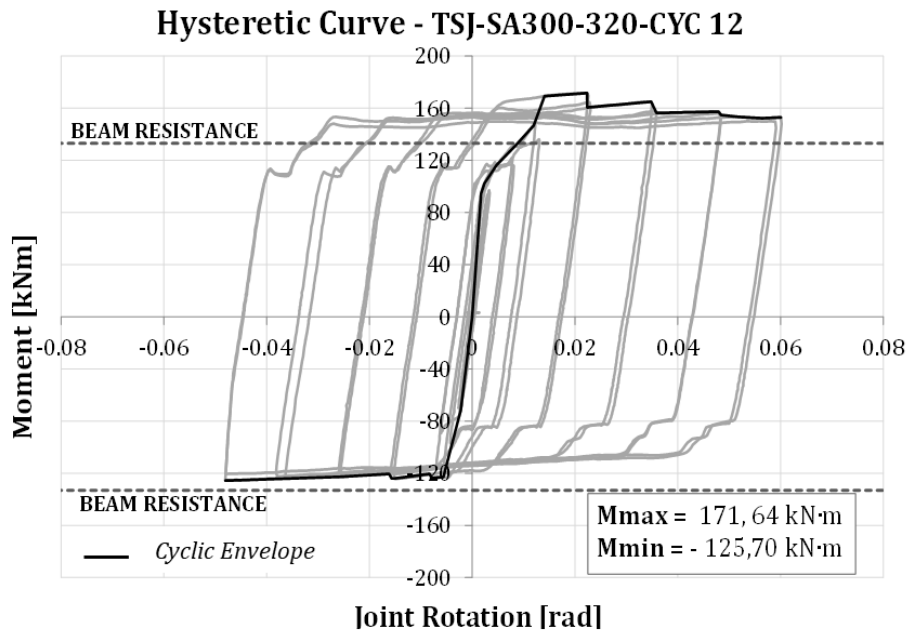


Figure 18: Force-Displacement response of the friction dampers

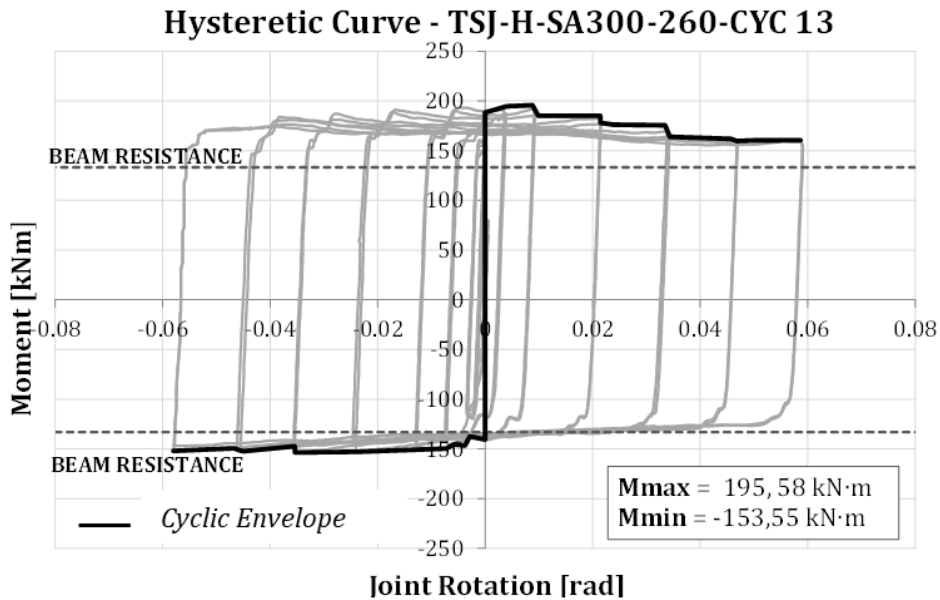
563

564

565 The most important feature of the proposed connection is that, as confirmed by the
 566 experimental results, it is able to provide a high dissipative capacity also under values of the
 567 rotation significantly greater than the minimum value, equal to 35 mrad, required by
 568 Eurocode 8 [1] for frames in High Ductility Class. Furthermore, it is possible to observe from
 569 Fig. 18 and Fig. 19 that the resistances of the joints and of the dampers approximately
 570 correspond to the design ones, confirming the accuracy of the design procedure previously
 571 described. Finally, it is very important to underline that the obtained flexural strength is
 572 greater than the plastic resistance of the connected beam, so that practically full-strength
 573 connections are obtained without providing any damage to the beam ends. This is highlighted
 574 in Fig.19 reporting with dashed lines the bending moment corresponding to the nominal
 575 beam resistance. In particular, it is worth to observe that even though no damage was
 576 detected in the elements of the connection or in the members, the nominal bending resistance
 577 of the beam evaluated at the level of the column face was equated or exceeded. This shows
 578 that with the proposed connection it is possible to obtain a wide and stable hysteretic
 579 behaviour with negligible damage, carrying the same forces that the beam would normally
 580 carry with a full-strength connection.



581



582

583

Figure 19: Moment-rotation curves of tested joints

584

585 **6. CONCLUSIONS**

586 The results of an experimental program devoted to evaluate the possibility to equip steel
 587 joints with friction dampers realized with pads coated with thermally sprayed aluminium
 588 have been presented. The main outcomes of the experimental programs can be summarized
 589 as follows:

- 590 • The frictional interface “thermally sprayed aluminium on steel” is characterized by
 591 good values of the kinematic friction coefficient. In fact, compared to other metallic or

- 592 rubber materials tested in a past experimental program under the same loading
593 conditions it is able to exhibit greater values of the friction coefficient;
- 594 • **The** thermally sprayed aluminium has, among the various advantages, the benefit to be
595 an economic material compared to rubbers or other metals typically used for
596 tribological applications such as brass;
 - 597 • **The** friction coefficient of the interface decreases as far as the pressure applied to the
598 interface increases. Therefore, in order to develop high values of the sliding force it is
599 advisable to limit the pressure applied on the frictional material, as an example by
600 increasing the number of the bolts thus allowing the reduction of their tightening
601 torque;
 - 602 • **The** results of the experimental program on the friction damper have shown that a
603 good balance between the initial value of the friction coefficient and the degradation of
604 the sliding force during a cyclic loading history can be reached with a thickness of
605 aluminium coating equal to 300 μm ;
 - 606 • **As** the bolt preloading has not been directly measured and monitored throughout the
607 tests, it is not possible to quantify in detail the actual value of the friction coefficient
608 and its evolution during the tests. Notwithstanding, the overall sliding resistance of the
609 damper is accurate as directly measured in the components' tests and derived as the
610 ratio between the sliding flexural resistance and the lever arm in the tests on beam-to-
611 column connections. This force is directly affected by the tightening torque;
 - 612 • **For** the above reasons, new experimental tests are currently in progress where the bolt
613 preloading is continuously measured by means of annular load cells.

614

615 **ACKNOWLEDGEMENTS**

616 The research activity herein presented has been supported by the European Community by
617 research grant RFSR-CT-2015-00022. The support of the European Commission within RFCS
618 Research & Innovation is gratefully acknowledged.

619

620 **REFERENCES**

- 621 1. CEN. Eurocode 8: Design of structures for earthquake resistance - Part 1: General
622 rules, seismic actions and rules for buildings; 2005a.

- 623 2. D'Aniello M., Tartaglia R., Costanzo S., Landolfo R. (2017). Seismic design of
624 extended stiffened end-plate joints in the framework of Eurocodes. Journal of
625 Constructional Steel Research, Volume 128, January 2017, Pages 512–527.
- 626 3. Piluso V, Rizzano G. Random Material Variability effects on Full-strength end-plate
627 Beam-to-Column Joints. Journal of Constructional Steel Research. 2007;63(5):658-
628 666.
- 629 4. Latour M, Rizzano G. Full Strength Design of Column Base Connections accounting
630 for Random Material Variability. Engineering Structures. 2013;48:458-471.
- 631 5. Mazzolani F, Piluso V. Theory and Design of Seismic Resistant Steel Frames.
632 London: E & FN Spon, an Imprint of Chapman & Hall; 1996.
- 633 6. D'Aniello M, Landolfo R, Piluso V, Rizzano G. Ultimate behavior of steel beams
634 under non-uniform bending. Journal of Constructional Steel Research.
635 2012;78:144-158.
- 636 7. Grecea D, Dinu F, Dubina D. Performance Criteria for MR Steel Frames in Seismic
637 Zones. Journal of Constructional Steel Research. 2004;60:739-749.
- 638 8. Carter CJ, Iwankiw N. Improved ductility in seismic steel moment frames with
639 dogbone connections. Journal of Constructional Steel Research. 1998;46(1-3):253.
- 640 9. Engelhardt MD, Winneberger T, Zekany AJ, Potyraaj TJ. Experimental investigation
641 of dogbone moment connections. Paper presented at: Proceedings of National Steel
642 Construction Conference, 1997; Chicago.
- 643 10. Montuori R., Nastri E., Piluso V., Troisi M. Influence of connection typology on
644 seismic response of MR-Frames with and without 'set-backs'. Earthquake
645 Engineering & Structural Dynamics. 2017; 46 (1), 5-25.
- 646 11. Montuori R., Nastri E., Piluso V., Advances in theory of plastic mechanism control:
647 closed form solution for MR-Frames. Earthquake Engineering & Structural
648 Dynamics. 2015; 44 (7), 1035-1054
- 649 12. Faella C, Montuori R, Piluso V, Rizzano G. Failure mode control: economy of semi-
650 rigid frames. Paper presented at: Proceedings of the XI European Conference on
651 Earthquake Engineering, 1998; Paris.
- 652 13. Tenchini A., D'Aniello M., Rebelo C., Landolfo R., da Silva L.S., Lima L. (2014).
653 Seismic performance of dual-steel moment resisting frames. Journal of

- 654 **Constructional Steel Research, Volume 101, October 2014, pp. 437-454.**
655 **DOI:10.1016/j.jcsr.2014.06.007**
- 656 **14. Cassiano D., D’Aniello M., Rebelo C., Landolfo R., da Silva L. (2016). Influence of**
657 **seismic design rules on the robustness of steel moment resisting frames. Steel and**
658 **Composite Structures, An International Journal, Volume 21, Number 3, , pp. 479-**
659 **500, June30 2016**
- 660 15. Faella C, Piluso V, Rizzano G. Structural Steel Semi-Rigid Connections. Boca Raton:
661 CRC Press; 2000.
- 662 16. CEN. Eurocode 3: Design of steel structures - Part 1-1: General rules and rules for
663 buildings; 2005b.
- 664 17. CEN. Eurocode 3: Design of steel structures - Part 1-8: Design of joints; 2005c.
- 665 **18. Cassiano D., D’Aniello M., Rebelo C., (2017) Parametric finite element analyses on**
666 **flush end-plate joints under column removal. Journal of Constructional Steel**
667 **Research, Volume 137, October 2017, Pages 77-92**
- 668 19. Iannone F, Latour M, Piluso V, Rizzano G. Experimental Analysis of Bolted Steel
669 Beam-to-Column Connections: Component Identification. Journal of Earthquake
670 Engineering. 2011;15(2):214-244.
- 671 20. Jaspart J, Demonceau J. European Design recommendations for simple joints in
672 steel structures. Journal of Constructional Steel Research. 2008;64/7(8):822-832.
- 673 21. Jaspart J, Demonceau J. Simple Connections. Publ.126 ed. Brussels: ECCS Press;
674 2009.
- 675 22. Castro JM, Elghazouli AY, Izzudin BA. Modelling of the panel zone in steel and
676 composite moment frames. Engineering Structures. 2005;27:129-144.
- 677 23. Bravo M, Herrera R. Performance under cyclic load of built-up T-stubs for Double T
678 moment connections. Journal of Constructional Steel Research. 2014;103:117-130.
- 679 24. Dubina D, Montreau N, Stratau A, Grecea D, Zaharia R. Testing program to evaluate
680 behavior of dual steel connections under monotonic and cyclic loading. Paper
681 presented at: Proceedings of the 5th European Conference on Steel and Composite
682 Structures, 2008; Graz, Austria.
- 683 25. Kim KD, Engelhardt MD. Monotonic and cyclic loading models for panel zones in
684 steel moment frames. Journal of Constructional Steel Research. 2002;58:605-635.

- 685 26. Saberi V, Gerami M, Kheyroddin A. Comparison of bolted end plate and T-stub
686 connection sensitivity to component thickness. *Journal of Constructional Steel*
687 *Research*. 2014;98:134-145.
- 688 27. Nogueiro P, Simoes da Silva L, Bento R, Simoes R. Calibration of Model Parameters
689 for the Cyclic Response of End-Plate Beam-to-Column Steel-Concrete Composite
690 Joints. *Journal of Steel and Composites Structures*. 2009;9(1):35-58.
- 691 28. Kim Y, Ryu H, Kang C. Hysteretic Behaviour of Moment Connections with Energy
692 Absorption Elements at Beam Bottom Flanges. Paper presented at: ICAS 2007,
693 2007; Oxford.
- 694 29. Latour M, Rizzano G. Experimental Behavior and Mechanical Modeling of
695 Dissipative T-Stub Connections. *Journal of Structural Engineering*.
696 2012;138(2):170-182.
- 697 30. Latour M, Rizzano G. Design of X-shaped double split tee joints accounting for
698 moment-shear interaction. *Journal of Constructional Steel Research*.
699 2015c;104:115-126.
- 700 31. Inoue K, Suita K, Takeuchi I, Chusilp P, Nakashima M, Zhou F. Seismic-Resistant
701 Weld-Free Steel Frame Buildings with Mechanical Joints and Hysteretic Dampers.
702 *Journal of the Structural Engineering, ASCE*. 2006;132(6):864-872.
- 703 32. Kishiki S, Yamada S, Suzuki K, Saeki E, Wada A. New Ductile Moment-Resisting
704 Connections Limiting Damage to Specific Elements at the Bottom Flange., 2006;
705 San Francisco.
- 706 33. Christopoulos C, Filiatrault A. Principles of Passive Supplemental Damping and
707 Seismic Isolation. Pavia: IUSS PRESS; 2006.
- 708 34. Soong TT, Spencer Jr BF. Supplemental Energy Dissipation: State-of-the-Art and
709 State-of-the-Practice. *Engineering Structures*. 2002;24:243-259.
- 710 35. Mualla I, Belev B. Seismic Response of Steel Frames Equiped with a New Friction
711 Damper Device Under Earthquake Excitation. *Engineering Structures*.
712 2002;24(3):365-371.
- 713 36. Oh S, Kim Y, Ryu H. Seismic Performance of Steel Structures with slit dampers.
714 *Engineering Structures*. 2009;31:1997-2008.

- 715 37. Latour M, Piluso V, Rizzano G. Experimental behaviour of friction T-stub beam-to-
716 column joints under cyclic loads. *Steel Construction* (1). 2013b.
- 717 38. Yan T, Popov E. Experimental and analytical studies of steel connections and
718 energy dissipators. Berkeley: Earthquake Engineering Research Center; 1995.
719 UCB/EERC-95/13.
- 720 39. Khoo H, Clifton G, Macrae G, Ramhormozian S. Proposed design models for the
721 asymmetric friction connection. *EARTHQUAKE ENGINEERING & STRUCTURAL*
722 *DYNAMICS*. December 2014;44(8):1309-1324.
- 723 40. Khoo H, Clifton C, Butterworth J, MacRae G, Gledhill S, Sidwell G. Development of
724 the self-centering Sliding Hinge Joint with friction ring springs. *Journal of*
725 *Constructional Steel Research*. 2012a;78:201-211.
- 726 41. Khoo H, Clifton J, Butterworth J, Macrae G. Experimental Study of Full-Scale Self-
727 Centering Sliding Hinge Joint Connections with Friction Ring Springs. *Journal of*
728 *Earthquake Engineering*. September 2013(17):972-997.
- 729 42. Borzouie J, Macrae G, Chase J, et al. Cyclic Performance of Asymmetric Friction
730 Connections with Grade 10.9 Bolts. *The Bridge and Structural Engineer*. March
731 2015;45(1).
- 732 43. Latour M, Piluso V, Rizzano G. Experimental analysis of innovative dissipative
733 bolted double split tee beam-to-column connections. *Steel Construction*. June
734 2011a;4(2):53-64.
- 735 44. Yeung S., Zhou H., Khoo H.H., Clifton G.C., MacRae G.A. Sliding shear capacities of
736 the Asymmetric Friction Connection. 2013 NZSEE Conference, April 26-28,
737 Wellington, 2013. Paper n. 27,
- 738 45. Butterworth J.W., Clifton G.C., Performance of Hierarchical Friction Dissipating
739 Joints in Moment Resisting Steel Frames. 12 World Conference on Earthquake
740 Engineering, Paper N. 718, 2000.
- 741 46. Latour M, Piluso V, Rizzano G. Experimental Analysis of Friction Materials for
742 supplemental damping devices. *Construction and Building Materials*. 2014b.
- 743 47. Latour M, Piluso V, Rizzano G. Free from damage beam-to-column joints: Testing
744 and design of DST connections with friction pads. *Engineering Structures*.
745 2015a;85:219-233.

- 746 48. Ono S, Nakahira K, Tsujioka S, Uno N. Energy Absorption Capacity of Thermally
747 Sprayed Aluminum Friction Dampers. Journal of Thermal Spray Technology.
748 September 1996;5(3).
- 749 49. Sato A, Kimura K, Suita K, Inoue K. Cyclic Test of High Strength Steel Beam-to-
750 Column Connection Composed with Knee-Brace Damper and Friction Damper
751 Connected by High Strength Bolts, 2009; Proceedings of the SEEBUS 2009. Kyoto,
752 Japan.
- 753 50. D'Aniello M., Cassiano D., Landolfo R., (2016) Monotonic and cyclic inelastic tensile
754 response of European preloadable GR10.9 bolt assemblies. Journal of
755 Constructional Steel Research, 124: 77-90.
- 756 51. D'Aniello M., Cassiano D., Landolfo R., (2017) Simplified criteria for finite element
757 modelling of European preloadable bolts. Steel and Composite Structures, An
758 International Journal Vol. 24, No. 6 (2017) 643-658
- 759 52. Heistermann C. Behaviour of Pretensioned Bolts in Friction Connections. Lulea:
760 Lulea University of Technology; 2011.
- 761 53. Schnorr. Handbook for Disc Springs. Heilbronn: Adolf Schnorr GmbH; 2003.
- 762 54. UNI-CEI-CNR. Costruzioni di acciaio. Istruzioni per il calcolo, l' esecuzione, il
763 collaudo e la manutenzione. Steel structures. Instructions of design, construction,
764 testing and maintenance.: UNI; 1988.
- 765 55. CEN. UNI EN 1090-2. Steel structures. Instructions of design, construction, testing
766 and maintenance. Steel structures. Instructions of design, construction, testing and
767 maintenance.; 2008.
- 768 56. Paciello A. Progettazione e analisi delle prestazioni sismiche di sistemi accoppiati
769 in acciaio con collegamenti di tipo "FREEDAM". MSc - Università degli Studi di
770 Salerno: Tesi di laurea in Ingegneria edile-architettura; 2015.
- 771 57. Heistermann C, Veljkovic M, Simoes R, Rebelo C, Simoes da Silva L. Design of slip
772 resistant lap joints with long open slotted holes. Journal of Constructional Steel
773 Research. 2012;82:223-233.
- 774 58. Kulak G, Fisher J, Struik J. Guide to design criteria for bolted and riveted joints:
775 Research Council on Structural Connections; 2001.
- 776 59. AISC. Seismic Provisions for Structural Steel Buildings. Chicago, Illinois; 2005.

- 777 60. Golondrino JC, MacRae G, Chase J, Rodgers G., Clifton GC. Velocity effects on the
778 behavior of asymmetrical friction connections (AFC). 8th STESSA Conference,
779 Shanghai, China, July 1-3, 2015
- 780 61. Ferrante Cavallaro, G., Latour, M., Francavilla, A.B., Piluso, V., Rizzano, G.
781 Standardised friction damper bolt assemblies time-related relaxation and installed
782 tension variability (2018) Journal of Constructional Steel Research, 141, pp. 145-
783 155.
- 784